Revision 1

Diffusion of phosphorus in olivine and molten basalt

E.B. Watson, D.J. Cherniak, M.E. Holycross
Department of Earth and Environmental Sciences
Rensselaer Polytechnic Institute
Troy, New York 12180 U.S.A.

Abstract

The diffusivity of phosphorus in San Carlos olivine (SCO) was measured at near-atmospheric pressure and 650°-850°C by in-diffusion of P from a surface powder source consisting of pre-reacted SCO and $AlPO_4$. The experiments were conducted in evacuated silica-glass ampoules at oxygen fugacities fixed by solid-state buffers, generally Ni-NiO but also including two experiments buffered at wüstite-magnetite. Phosphorus uptake profiles were characterized by Rutherford backscattering spectroscopy (RBS) and nuclear reaction analysis (NRA). The temperature dependence of P diffusion in SCO conforms to the expected Arrhenius relation $D = D_0 \exp(-E_a/RT)$, where the constants are as follows: $\log(D_0, m^2/s) = -10.06 \pm 0.80$ and $E_a = 229 \pm 16$ kJ/mol. These values characterize P as a relatively slow diffuser in olivine—slower by about an order of magnitude than Cr and Ca at basalt near-liquidus temperatures—but substantially faster than Si.

With a view toward modeling P uptake during rapid growth of natural olivines, P diffusion was also characterized in dry MORB basalt melt over the temperature range 1250°-1500°C at 1 GPa, using traditional diffusion couples contained in graphite. Phosphorus diffusion profiles in the quenched and depressurized samples were quantified by laser-ablation ICP/MS.

Phosphorus diffusion in basaltic melt is similar to that of Si, with $\log(D_0, m^2/s) = -6.30 \pm 0.7$ and $E_a = 147 \pm 22$ kJ/mol.

The new data for P diffusion in olivine and basalt melt can be used to explore the acquisition of fine-scale zoning in natural olivine phenocrysts through kinetic models, as well as the survival of P zoning in olivine with time spent at elevated temperature. Models of growth entrapment of a P-enriched near-surface layer in the olivine lattice indicate that crystal growth at plausible sustained rates is indeed likely to result in regions of anomalously high P content in the resulting crystal. Phosphorus concentrations above the equilibrium partitioning value can also result from development of a diffusive boundary layer in the melt against a rapidly-growing crystal, but this mechanism is ineffective at typical sustained olivine growth rates, requiring dendrite-forming growth speeds. Preservation of P zoning on the scale of a few microns apparently requires cooling within a few months of formation of the zoning.

INTRODUCTION

Because of its abundance in Earth's mantle and crust and in some meteorites, magnesian olivine has been the subject of numerous diffusion studies, targeting both major components (Mg, Fe, Si, O) and trace elements (H, Li, Be, Al, Ca, Ti, Cr, Mn, Co, Ni, Sr, REE; see summary by Chakraborty 2010 and references therein; Spandler et al. 2007; Spandler and O'Neill 2009; Cherniak 2010). Conspicuously missing from the group of elements whose diffusion properties have been characterized is phosphorus. The lack of P diffusion data is a significant shortcoming given the complex P zoning patterns noted in some terrestrial and meteorite olivines (Milman-Barris et al. 2008; Mallman et al. 2009; Tschegg et al. 2010; Sakyi et al. 2012; McKibbin et al.

2013; Welsch et al. 2013; 2014): the formation and persistence of this sometimes delicate zoning may be related in some way to ineffective P diffusion. Here we address this gap in diffusion information by measuring the diffusivity of P in San Carlos olivine (Fo_{90}) at near-atmospheric pressure, 650-850°C and oxygen fugacities buffered at Ni-NiO and FeO-Fe_3O_4.

A second goal of this effort was to incorporate the new diffusion measurements into numerical models of olivine crystal growth that might shed light on the remarkable P zoning patterns observed in some natural and synthetic olivines. Some of these models require knowledge of diffusion in the growth medium, so we also characterized chemical diffusion of P in basaltic melt as a function of temperature over the range 1250°-1500°C. To our knowledge, P diffusion in basaltic melt has not been characterized thoroughly at temperatures directly relevant to natural systems. Four data points spanning ~1250°-1450°C are available in the combined studies of Lundstrom (2003) and Baker (2008), but one of these studies involved complex diffusion phenomena—e.g., co-diffusion of Ca and P away from dissolving apatite in the study of Baker (2008). The previous results are not in good agreement, which complicates the choice of diffusivities for modeling purposes.

EXPERIMENTS AND ANALYSES

Materials and preparation

The P diffusion experiments on olivine were conducted using oriented slabs (~1×2×3 mm) of San Carlos olivine (SCO) cut from ~cm-sized pieces. The slabs were ground and polished on one face, beginning with SiC grit (down to 600), followed by 1-μm α-alumina, and finishing with at least 4 hours of polishing with colloidal silica. This procedure is described in more detail by

Cherniak et al. (2014), who also demonstrated that olivine crystal surfaces prepared in this way exhibit no mechanical damage observable at the ~10 nm scale. Most experiments were conducted on SCO slabs cut parallel to the b crystallographic axis, but some experiments were also conducted on sections cut parallel to the c axis in order to evaluate possible anisotropy of P diffusion.

Diffusion experiments on molten basalt were conducted using synthetic mid-ocean ridge basalt (N-MORB) modeled on a natural material commonly used in the RPI laboratory and referred to as "SUNY MORB" (this basalt was developed as a standard by Prof. A. Miyashiro of SUNY Albany in the 1970s). Two synthetic MORBs, one containing no P and the other ~0.6 wt% P_2O_5, were prepared by from oxide and mineral powders. These materials constituted the two halves of simple diffusion couples, prepared as described below.

Experimental procedures

San Carlos olivine. The experiments on SCO were conducted using the powder-source method (Watson and Dohmen 2010) in evacuated silica glass ampoules, with the oxygen fugacity controlled by solid-state buffers (usually Ni-NiO, but including two experiments at wüstite-magnetite; see Table 1 and Figure 1). For most experiments, the powder source for P was a finely-ground, 60:40 (wt) mixture of SCO and $AlPO_4$ that had been pre-reacted, in vacuo, at 900°C for 16h. The rationale behind the choice of this source is that P^{5+} sometimes enters the olivine lattice via the coupled substitution $P^{5+} + Al^{3+}$(or Cr^{3+}) = $2Si^{4+}$ (see Milman-Barris et al. 2008). It seemed improbable that Al diffusion would rate-limit diffusive uptake of P in SCO in our experiments (simplistically speaking, this would require slower diffusion of a small 3+ ion than a small 5+ ion), but we anticipated that Al^{3+} might be required for P^{5+} to enter the olivine

lattice at all (in the end this proved not be the case, as concluded by Mallman et al. 2009 and McKibbin et al. 2013; see section "Analysis" section).

A second P diffusion source was prepared by pre-reacting ground San Carlos lherzolite with $AlPO_4$, also in 60:40 proportions. This alternative source was used in one experiment to explore the possibility that silica activity might influence P uptake and diffusion in SCO; the strategy was, effectively, to return the SCO slab to its original host assemblage (+ $AlPO_4$) for at least one experiment.

The SiO_2 ampoules were suspended in wire-wound, 1-atm furnaces, with temperature control to better than $\pm 2^{\circ}C$. The workable temperature range for the experiments was 650-850°C, the lower limit being determined by the slow diffusion of P and the need to generate diffusive-uptake profiles of at least 30-40 nm for accurate characterization (the longest experiments were over 2 months in duration). The effective upper temperature limit of the experiments was ~850°C. Above this temperature, the polished SCO surface in contact with the source underwent roughening during the experiment that degraded the quality of the depth profiles [see section 2.3 for analytical details; see also Watson and Dohmen (2010) for a general discussion of the effects of surface roughening on ion-beam analysis]. A time series of 4 experiments was conducted at 825°C with durations varying over nearly an order of magnitude (70 ~ 670 hours) in order to confirm that the measured diffusivities are independent of experiment duration. Pertinent information for the SCO experiments is summarized in Table 1a.

Basaltic melt. Starting materials for the basalt experiments were prepared from oxide and silicate powders mixed to yield the following bulk composition (wt%): SiO_2 = 50.0; TiO_2 =

1.6; Al_2O_3 = 16.0; FeO = 7.6; Fe_2O_3 = 2.0; MgO = 8.5; CaO = 10.8; Na_2O = 3.0; K_2O = 0.2; MnO = 0.2. A second composition containing ~0.6 wt% P_2O_5 was prepared by including $Ca_3(PO_4)_2$ in the mixture, maintaining the same proportions of all other components. The powders were ground in agate under ethanol, dried thoroughly, loaded into graphite capsules in aliquots of ~200 mg, and fused in the piston-cylinder at 1300°C and 1 GPa for 2 hours. The quenched glasses were broken out of graphite capsules, crushed and ground under ethanol. After quenching and depressurization, the "high-P" and P-free glasses were recovered from the synthesis capsules and ground to fine powders for packing in a new graphite capsule as two halves of a diffusion couple, with the "high-P" glass on the bottom. The diffusion couple capsules were ~3 mm in I.D., with pre-compression length of ~8 mm. These were displaced 0.25 mm downward from the vertical center of the graphite heater to decrease the chances of convection (this measure ensures that the melt is slightly warmer at the top, but the estimated T difference is no more than 5°; Watson et al. 2002). The couples were run in a 3/4" piston-cylinder assembly that is standard in the RPI lab for dry experiments at high temperature (Figure 2). The couples were cold pressurized to ~1 GPa and ramped up to run temperature (1250° - 1500°C) at 100° - 400°C/min, depending on anticipated duration. A final pressure adjustment was made when run temperature was reached. The samples were quenched by turning off the power to the graphite heater, which resulted in cooling to 100°C within ~20 s. The quenched and depressurized diffusion couples were recovered intact from the piston-cylinder assembly, "potted" in epoxy, ground to expose the glass, and vacuum-impregnated with epoxy. The mounts were then polished progressively with SiC paper (240-400-600 grit), followed by 1-μm alumina, and finished with colloidal silica in preparation for laser-ablation

ICP/MS analysis. See Table 1b for a summary of basalt diffusion experiment conditions and durations. Five runs of differing duration (90 - 5400s) were made at 1300°C to confirm that the P profiles began as concentration steps (90-s run) and that the recovered diffusivities were reproducible and independent of experiment duration.

Analysis

Olivine. After quenching the olivine diffusion experiments, the polished surfaces of the samples were cleaned by gentle brushing with a plastic implement, followed by sonication in alcohol for 10-30 minutes. Following this cleaning step, the surfaces of some samples were imaged by SEM, which revealed little evidence of residual adhering source material. The surfaces were then depth-profiled for phosphorus using both Rutherford backscattering spectroscopy (RBS) and nuclear reaction analysis (NRA).

RBS has been used in many of our diffusion studies (e.g., Cherniak and Watson 1994; Cherniak 2010) and the experimental and analytical approach used here is similar to that taken in our previous work. Analyses employed $^{4}He^{+}$ beams having energies of 2 or 3 MeV, with beam spot size typically ~1mm^2. Spectra were converted to phosphorus concentration profiles using procedures outlined in publications cited above.

The RBS profiles of phosphorus measured in the olivine following diffusion anneals were fit with a model to determine the diffusion coefficients (*D*). Diffusion was modeled as simple one-dimensional, concentration independent diffusion in a semi-infinite medium with a source reservoir maintained at constant concentration. The rationale for the use of this model has been discussed in previous studies (e.g., Cherniak and Watson 1994) and is used by many researchers. Diffusivities were evaluated by plotting the inverse of the error function (i.e., *erf*

153 $^{1}((C_o - C(x,t))/C_o))$ vs. depth (x) in the sample. A straight line of slope $(4Dt)^{-1/2}$ will result if the
154 data satisfy the conditions of the model. The surface concentration of diffusant, C_o, is
155 independently determined by iteratively varying its value until the intercept of the line
156 converges on zero. Error estimates for each data point were used to evaluate the uncertainties
157 in the diffusivities determined from the fits to the model. Uncertainties in concentration come
158 from counting statistics; uncertainties in depth arise from detector resolution and energy
159 spread of the analyzing ion beam.

160 In addition to analyses by RBS, phosphorus was also profiled in samples using nuclear
161 reaction analysis (NRA) with the reaction $^{31}P(\alpha,p)^{34}S$ (McIntyre et al. 1988). The 3.640 MeV
162 resonance of the reaction was used, with depth profiling accomplished by increasing beam
163 energy by steps of 2 to 5 keV. Protons produced in the (α,p) reaction were detected with a solid
164 state surface barrier detector (as used for the RBS measurements) covered with 7.5 μm Kapton
165 foil to stop backscattered alpha particles. For analyses at each energy step, a spectrum from an
166 untreated specimen of the olivine was taken to determine background signals in the energy
167 range of the protons produced in the $^{31}P(\alpha,p)^{34}S$ reaction. Specimens of apatite and monazite
168 were also analyzed as standards. Phosphorus profiles obtained from RBS and NRA
169 measurements are in good agreement and yield diffusivities that are the same within
170 uncertainty. Typical RBS profiles are shown in Figure 3.

171 To assess the potential substitution mechanisms for P involving Al, we measured Al in some
172 of the olivine samples using the nuclear reaction $^{27}Al(p,\gamma)^{28}Si$ (Sautter et al. 1988; Cherniak and
173 Watson 1994; Cherniak 1995). The 992 keV resonance of the reaction was used, with energy
174 steps for the incident proton beam of 0.5 to a few keV for depth profiling. Gamma rays

produced in the reaction were detected with a bismuth germanate (BGO) detector. As with the phosphorus profiling, an untreated sample of olivine was analyzed at each energy step to assess backgrounds in gamma spectra in the energy region of interest. Gamma spectra of Al foil were collected as standards for conversion of gamma yields into Al concentrations in olivine samples. Depth scales for the Al profiles were calculated from the energy difference between the incident proton beam and the resonance energy, and by the stopping power (energy loss of the protons as a function of depth in the material; e.g., Cherniak and Lanford 2001); stopping powers for protons in the olivine matrix over the energy range employed in depth profiling were obtained from the software SRIM (Ziegler and Biersack, 2006).

The results from Al profiling by NRA reveal profile lengths comparable to those for P, but the concentration of Al always much lower, ranging from a few percent to ~15% of P levels. This observation confirms that Al co-substitution with P is not required for charge compensation of P entry into olivine (see Mallman et al. 2009; McKibbin et al. 2013), even if the diffusivities of the two elements appear to be similar.

MORB melt. Phosphorus concentration measurements on the polished diffusion couples were obtained using RPI's laser-ablation ICP-MS, which consists of a Photon Machines Analyte 193 laser-ablation workstation and a Bruker 820-MS inductively coupled plasma quadrupole mass spectrometer. Analytical profiles were generated by stepping a 40-μm square spot size along the couple axis at 80- μm intervals. Samples were ablated for 30 s at each spot, bracketed by 15 s during which the shutter remained closed to measure the background. NIST 612 was used as the standard reference for glass analyses. Data were reduced using Iolite software for Igor Pro. Silicon-29 was used as the internal standard reference in the trace

element data reduction scheme. Representative P profiles in the quenched melts are shown in Figure 4. Diffusivities were obtained from the analytical profiles by fitting the data to the solution to the non-steady state diffusion equation for an infinite diffusion couple (see Figure 4), using Origin® v. 8.6. Uncertainties on the reported diffusivities (±2 s.e.) are based on the residuals of the fits to the diffusion couple model.

RESULTS AND DISCUSSION

Phosphorus diffusion in olivine

Measured diffusivities for phosphorus in San Carlos olivine are summarized in Table 1a and in Figure 5 as a plot of logD vs. 1/T. The data form a coherent array, corresponding to the expected dependence of D upon temperature: $D = D_0 \exp(-E_a/RT)$, where D_0 is the pre-exponential factor (m^2/s), E_a is the activation energy for diffusion (J/mol), R is the gas constant (J/K·mol) and T is temperature in kelvins. None of the other variables explored for possible effects on P diffusion—oxygen fugacity, crystallographic direction and P source—appears to play a significant role. The two experiments run at an oxygen fugacity buffered at wüstite-magnetite (WM) yield diffusivities slightly higher than those run at NNO at similar temperatures, but the 2-σ error bars overlap so these cannot be regarded as significantly different. Similarly, there is no statistically significant difference in results from experiments involving diffusion parallel to the b and c crystallographic axes, nor does the incorporation of a peridotite assemblage in the P source (as opposed to simply ground olivine) appear to affect the outcome. For this reason we regressed all 16 diffusivity values as single data set, which yielded the following Arrhenius parameters: $\log(D_0, m^2/s) = -10.06 \pm 0.80$; $E_a = 229 \pm 16$ kJ/mol.

Figure 6 shows the results of the time series conducted at 825°C. No significant change in D is apparent with increasing run duration, which strongly supports the case for lattice-diffusion control of P transport in San Carlos olivine (if fast-paths were involved, for example, fitting the raw data to the simple error-function solution would not result in a time-invariant D). As is commonly the case in the time series we include in all our diffusion studies, the shortest run durations tend to yield diffusivities slightly higher than the time-averaged value. This is because the shortest profiles (~30 nm) challenge the ~5- to 10-nm depth resolution of RBS. Minor analytical broadening of the profile results, which leads to a slightly elevated apparent diffusivity. It is clear from Figure 6 that this effect is small, and any impact on the overall results is negligible because we strive for profile lengths exceeding 50 nm.

We are not reporting detailed data for aluminum in this paper because the Al concentrations in our samples were too low for accurate characterization. We can conclude, nevertheless, that the diffusion characteristics of Al in olivine are broadly similar to those of P. As noted in the "Analysis" section, our results indicate that Al is not required for entry of P into the olivine lattice, even though P sometimes correlates with Al (or Cr) in natural olivines (Milman-Barris et al. 2008). This raises the question of exactly what substitution is involved when P diffuses into San Carlos olivine from our $AlPO_4$ source. Unfortunately, our analytical methods are not well suited to characterization of minor diffusive loss of a major element or elements (Si, Mg, Fe) that might accompany uptake of P. Some of our RBS spectra show slight rounding of the Si edge that might be indicative of minor Si loss from the near-surface, but these features are neither universal nor quantifiable in a meaningful way. It seems clear, in any case, that Si mobility does not rate-limit P migration, given that P diffuses substantially faster

than Si in olivine (section 4.1). Mallman et al. (2009) noted correlations of P with Li or Na, but these elements were not present in our P source.

Comparison with other elements in olivine

Phosphorus has been regarded as a slow-diffusing element in olivine because phosphorus zoning is preserved in situations where other elements appear to have been homogenized by diffusion (Spandler et al. 2007; Milman-Barris et al. 2008; Mallman et al. 2009). To our knowledge, there exists just one previous estimate of the diffusivity of P in olivine, which is that of Spandler et al. (2007; see also Mallman et al. 2009) based on an attempt to homogenize fine-scale P zoning in a natural olivine by heat treatment. No mobilization of P detectable by backscattered-electron imaging was observed after 30 days at 1300°C, leading the authors to conclude that the diffusivity of P is $<10^{-18}$ m^2/s at this temperature. Interestingly, this value maximum value falls essentially on top of the up-temperature extrapolation our Arrhenius line, within the uncertainty in our line (Figure 7). In this respect, we agree with the common wisdom that P diffusion in olivine is slow, but our new data also indicate that P is nevertheless much faster diffusing than Si (a surprise to us), and slightly faster than oxygen under dry conditions. Phosphorus also appears to diffuse somewhat faster than the rare earths as reported by Cherniak (2010) and Remmert et al. (2008), although Spandler et al. (2007) obtained much higher REE diffusivities (see Figure 7). Our data place P diffusion in San Carlos olivine about an order of magnitude slower than Ca and roughly 2-4 orders of magnitude slower than Fe-Mg interdiffusion in olivines of similar composition [the difference in the latter case depends upon oxygen fugacity, which affects Fe-Mg interdiffusion (Chakraborty 1997)]. Because P is a highly-charged (5+) cation, we anticipated a very high activation energy for diffusion—perhaps

exceeding that of Si—but our value of ~230 kJ/mol is more similar to those for diffusion of divalent and univalent cations and metal vacancies (Figure 7).

A major conclusion of our study is that P in olivine cannot be regarded as immobile for all T-t histories. This could be considered an undesirable outcome because it means that P zoning is not universally reliable as an immovable marker against which diffusion profiles of other, more mobile, diffusants can be evaluated. In natural crystals that are grown and cooled relatively quickly (e.g., Welsch et al. 2014), P diffusion will be very limited, but slower cooling may result in some diffusive relaxation of initially steep profiles. Viewed in a positive light, some diffusion can be better than none because it opens up possibilities for modeling thermal histories that are not available for an essentially immobile element. Examples are discussed in the "Diffusive relaxation" section.

Phosphorus diffusion in MORB melt

Our measured diffusivities for P in molten basalt are shown in Figure 8 for the temperature range 1250°-1500°C (see also Table 1b). As in the case of the olivine data, the basalt data form a coherent array, with Arrhenius parameters as follows: $\log(D_0, m^2/s) = -6.30 \pm 0.7$ and $E_a = 147 \pm 22$ kJ/mol. In contrast to the case of San Carlos olivine, the P diffusion data for basaltic melt were obtained near the temperature range of direct relevance to natural systems, so the somewhat larger uncertainty in Arrhenius parameters will have little impact on choice of diffusivities for modeling purposes. Figure 9 shows the results of a time series at 1300°C, which demonstrates that the recovered P diffusivity is independent of experiment duration.

Included in Figure 8 are data from previous studies for diffusion of both P and Si in broadly basaltic melts. Little difference between diffusion of P and Si at near-liquidus temperatures of generally basaltic melts is indicated. However, our new Arrhenius law for P is displaced upward from that of Baker (2008) by roughly an order of magnitude, and our activation energy is lower.

GEOCHEMICAL IMPLICATIONS AND APPLICATIONS

Origin of fine-scale phosphorus zoning in olivine

Recent studies by Milman-Barris et al. (2008) and by Welsch et al. (2014) have documented delicate P zoning features in natural olivines from volcanic rocks and experimental run products. This zoning is locally oscillatory in nature, on a length scale of a few microns, and includes excursions to P concentrations well above probable equilibrium values. For these reasons, the authors attributed the fine-scale zoning to kinetic influences during the growth of the host crystal, logically ruling out the likelihood of "external forcings"—i.e., short time-scale variations in magmatic conditions leading to fluctuations in P partitioning between olivine and melt. Milman-Barris et al. (2008), for example, concluded that oscillatory zoning of P in olivine phenocrysts and in their experimental run products is due to "solute trapping" as a consequence of rapid crystal growth from the melt. Although mechanistically vague as a descriptive term, solute trapping has been addressed extensively in the materials science literature using highly sophisticated approaches, generally with reference to simple alloy systems—and to crystal growth rates that are impossibly high for geological systems (e.g., m/s; see Aziz 1982; 1984;1996; Ahmad 1998; Galenko 2002; Lebedev et al. 2010). The general idea is that impurities near the crystal/melt interface become incorporated (trapped) in the crystal lattice at concentrations exceeding the equilibrium value when the growth rate outpaces the

ability of the impurities to diffuse away from the interface during growth. For the present purposes (and for geological systems) it is useful to divide near-surface kinetic phenomena leading to solute trapping into those that might occur in a diffusive boundary layer of melt against the crystal and those controlled by the near-surface properties of the crystal itself. This distinction is appropriate in geological systems because there exist natural examples of solute trapping that occurred at growth rates demonstrably too low to allow development of a diffusive boundary layer in the growth medium—e.g., sectoral and oscillatory zoning in zircons, among many others. This observation indicates control of solute trapping by transport in the crystal lattice itself, which means that the effect can operate independently of a melt boundary layer and at very low growth rates (zircon growth rates fall between 10^{-15} and 10^{-20} m/s; Watson 1996). Phosphorus zoning in olivine has characteristics in common with rare-earth zoning in zircon, but olivine crystals can grow substantially faster than zircons, so control by either a melt boundary layer or the crystal near-surface (or both) seems possible, as noted by Milman-Barris et al. (2008). The new data presented here for P diffusion in olivine and melt enable assessment of both possibilities.

Diffusive boundary layer in the melt. The development of diffusive boundary layers (DBLs) in melts against rapidly-growing crystals has been of interest to researchers in physics and materials science for 100 years (e.g., Schmoluchowski 1915; Tiller et al. 1953; Smith et al. 1955). The basic idea is that incompatible elements accumulate (or compatible elements are depleted) in advance of a moving crystal interface because diffusion in the growth medium is too slow to maintain uniform concentrations. Albarède and Bottinga (1972) first introduced this phenomenon to the geoscience community in the context of trace-element uptake in

rapidly growing phenocrysts. Watson and Müller (2009) extended the treatment to more relevant spherical geometries and to dynamic systems in which motion of the growing crystal relative to the host melt limits the extent of boundary-layer development. Concerning the behavior specifically of incompatible phosphorus in diffusive boundary layers against growing phenocrysts, Green and Watson (1982) cited rapid crystal growth of plagioclase as the probable cause of local apatite saturation in the contacting melt and consequent incorporation of minute apatite inclusions in the plagioclase (see also Harrison and Watson 1984; Bacon 1989). Milman-Barris et al. (2008) suggested that this phenomenon may be the cause of fine-scale zoning of P in olivine phenocrysts: if P is a slow diffuser in the melt, a transient interval of rapid olivine growth could result in a "pile-up" of incompatible P in the melt against the olivine and consequent rise of P concentration in the olivine, assuming equilibrium partitioning at the interface. Phosphorus diffusion data specifically for basaltic melts were not available to Milman-Barris et al. (2008), so they cited the study of Harrison and Watson (1984) on P diffusion in hydrous felsic melts as a confirmation that P diffusion in melts is slow. Quantitative calculations would have been risky at that time because of the questionable relevance to mafic systems of the (wet) felsic melt composition and low temperatures of the Harrison and Watson (1984) study. Baker (2008) characterized P diffusion in molten hawaiite specifically to evaluate the possibility that boundary-layer effects might influence the P content of melt inclusions formed by rapid growth of plagioclase and pyroxene (the answer is yes, but the deviation from equilibrium is more subtle than some P zoning features in olivine phenocrysts). Our new data for P diffusion in molten MORB basalt—which differ significantly from Baker's results for hawaiite—provide new constraints on models of P uptake in olivine during rapid crystal growth.

Figure 10 illustrates P uptake in olivine from a diffusive boundary layer in the melt produced by brief periods of rapid olivine growth at rates (V) of 10^{-8}, 10^{-7} and 10^{-6} m/s, assuming a temperature of 1215°C (where the diffusivity of P in the melt is 3.5×10^{-12} m^2/s). These results suggest that olivine growth at rates < 10^{-8} m/s has little effect on P uptake. However, growth at rates associated with dendrite formation ($\geq10^{-7}$ m/s; Jambon et al. 1992) can result in P concentrations in olivine significantly above equilibrium values—by a factor of 3 or 4 for $V \approx 10^{-6}$ m/s.

Near-surface effects in the crystal. As noted above, numerous papers in the materials science literature address the topic of "solute trapping," which is broadly defined as the uptake of impurities in crystals in excess of equilibrium levels as a consequence of rapid crystal growth (see, e.g., Aziz 1982; 1984; 1996; Ahmad 1998; Galenko 2002; Lebedev et al. 2010). Watson and Liang (1995) introduced a simple "growth entrapment" model (GEM) that differs in fundamental ways from metallurgical models in that it targets non-equilibrium effects that can operate at geologically plausible growth rates (see also Watson 1996; 2004; Lanzillo et al. 2014). Rather than focusing on dynamical effects at the crystal/melt interface or in immediately contacting melt, the governing kinetics of the growth entrapment model are localized to the crystal lattice where diffusion is relatively ineffective in leveling chemical potential gradients. Following Tiller and Ahn (1980), Watson and Liang (1995) postulated the existence of an *equilibrium* concentration anomaly in the near-surface of the crystal (but fully within the lattice) that decreases steeply (exponentially) toward the crystal interior (Figure 11). In most cases the anomaly would manifest as a high concentration of an incompatible element—e.g., P in olivine or Ti in quartz (Lanzillo et al. 2014)—but near-surface equilibrium

371 depletion is also possible (e.g., Pitters et al. 2012; see also Watson 2004). The chemical
372 anomaly is of little consequence to the overall composition of a static crystal, but when the
373 interface moves (as during growth) the anomalous near-surface region can be "captured" (i.e.,
374 become part of the crystal) if lattice diffusion is too slow to maintain bulk equilibrium. Growth
375 entrapment thus depends on the competition between crystal growth (which tends to bury the
376 near-surface anomaly) and diffusion (which works to disperse the anomaly). In order to explain
377 the systematics of apparent growth entrapment in calcite, Watson (2004) later postulated that
378 the diffusivity of the impurity of interest must depend on proximity to the surface over a
379 distance of ~ 1 nm. This surface-proximity effect on lattice diffusion was recently confirmed for
380 Ti diffusion in quartz through molecular dynamics simulations (Lanzillo et al. 2014): after
381 reproducing the activation energy E_a for Ti diffusion measured by Cherniak et al. (2007), these
382 authors showed that E_a drops by a factor of 2 approaching the quartz surface from a depth of 2
383 or 3 polyhedral layers. The Lanzillo et al. (2014) molecular dynamics simulations did not yield
384 absolute values for the near-surface diffusivity, so it is not clear whether it converges with the
385 bulk-lattice diffusivity at high temperature; however, the bulk-lattice value places a lower
386 bound on the near-surface diffusivity.

387 Modified to include depth-dependent diffusion (Watson 2004), the growth-entrapment
388 equation of Watson and Liang (1995) is:

389 $$\frac{\partial C_i}{\partial t} = \frac{\partial}{\partial z}\left\{\left[D_i \frac{\partial C_i}{\partial z}\right] - \frac{\ln F_s}{l}\left[C_i D_i \exp\left(\frac{z}{l}\right)\right]\right\} + V\frac{\partial C_i}{\partial z} \quad (1)$$

where C_i is the concentration of the impurity of interest at time t and distance z from the crystal surface (at z=0), V is the linear rate of advancement of the crystal/melt interface (i.e., the growth rate), D_i is the diffusivity of i in the lattice and l is the half-width of the equilibrium concentration anomaly (Figure 11). The parameter F_S represents the ratio of the equilibrium surface concentration to the bulk-lattice concentration—in effect, a surface/bulk-lattice partition coefficient. For assumed values of V, D_i, F_S and l, numerical simulations based on equation 1 yield C_i-x profiles in the crystal resulting from growth for a specified time period (Figure 12). The concentration plateaus in the shaded region of Figure 12 show the effectiveness of growth entrapment, with 100% indicating totally efficient capture of the anomalous surface composition represented by the value of F_S (see Figure 11). An entrapment efficiency of 50% results in a concentration plateau halfway between the true equilibrium composition of the crystal and F_S (Figure 12).

Diffusivity values for P in olivine calculated from our Arrhenius parameters can be used to evaluate growth-entrapment effectiveness based on equation 1, with the important caveat that diffusion in the outermost polyhedral layers critical to the phenomenon of growth entrapment could be significantly faster than the bulk-lattice values measured in this study (growth entrapment calculations based on bulk-lattice diffusivities will maximize entrapment effectiveness). We ran numerical simulations of P entrapment in olivine for a wide range of growth rates at temperatures of 1100°, 1200° and 1300°C, assuming F_S = 10 and l = 0.5 nm. The value of F_S is the least well constrained of all the assumed parameters, and entrapment efficiency does depend on F_S (Watson and Liang 1995). A value of 10 is considered plausible given the range of P concentrations observed in the fine-scale zoning described by Milman-

Barris et al. (2008), and given also that Lanzillo et al. (2014) estimated F_S for Ti in the quartz near-surface to be in the range of 12-18, depending on the specific crystal facet under consideration. The value of 0.5 nm for the half-width of the P-enriched region (l) is regarded as fairly robust because numerous minerals investigated to date by x-ray reflectivity exhibit near-surface lattice relaxation at this scale (see, e.g., Fenter et al. 2000a;b; 2001; 2003; Schlegel et al. 2002; Zhang eta l. 2007; Catalano et al. 2009). The same length scale also emerged from the Lanzillo et al. (2014) MD calculations for quartz.

Figure 13 shows growth-entrapment outcomes from equation 1 for $V = 10^{-11}$ to 10^{-6} m/s. The plotted points represent plateau levels (as in Figure 12) resulting from growth at the rates specified on the horizontal axis (see inset of Figure 13). In general, the concentration plateaus develop after only a few tens of nanometers growth at most (much less for the higher growth rates). Included in the figure is a shaded region indicating the range of sustained natural growth rates from the literature (e.g., Maaloe 2011), which seem to be bounded at the high end at ~5×10^{-9} m/s. Intermittent dendritic growth can occur at much faster rates—up to 6×10^{-7} m/s according to Jambon et al. (1992). The broad conclusion from this figure is that growth entrapment of P in olivine at levels several times the equilibrium concentration is plausible at the higher end of the time-averaged crystal growth rates believed to apply to natural systems (3×10^{-10} - 5×10^{-9} m/s). Growth "spurts" at still higher rates (up to 6×10^{-7} m/s; Jambon et al. 1992) certainly could result in the generally concentric and skeletal fine-scale zoning documented so effectively by Milman-Barris et al. (2008) and Welsch et al. (2014). These authors also noted sector zoning in some natural olivines, and given the facet-specific origin of sector zoning (Dowty 1977; Watson and Liang 1995), it seems inescapable that at least some P

zoning in olivine owes its existence to a mechanism like that embodied in equation 1. Anomalous concentrations arising from diffusive boundary layers in the melt should affect all surfaces equally unless individual facets grow at markedly different rates.

Note that lower temperatures favor P entrapment during growth at a specified rate due to more sluggish P diffusion in the olivine lattice; a negative temperature excursion might also promote faster olivine growth as a consequence of undercooling.

Diffusive relaxation of phosphorus zoning in olivine

In addition to the delicate zoning features documented by Milman-Barris et al. (2008) and Welsch et al. (2014), more subdued P zoning has been described by Mallman et al. (2009) in olivines from spinel peridotites. Our new data for P diffusion in olivine can be used to explore the post-formation holding times and cooling rates required for preservation of both fine- and coarse-scale zoning features.

Milman-Barris et al. (2008) documented fine-scale zoning of P in igneous olivines from a variety of rock types and settings—hosted mainly by basalts, but also including phenocrysts from more silicic calcalkaline rocks, a martian meteorite, and crystals grown in the laboratory. In the natural samples examined, the authors noted P levels in natural olivines varying from <0.01 wt% to as high as 0.4 wt% over distances as small as a few microns, while Mg and Fe levels remained constant over the same distance. Apparently, the faster-diffusing elements (Mg and Fe) were either uniform from the beginning or diffusively homogenized after the event(s) that led to formation of P zoning. In general, the preservation of fine-scale zoning in phenocrysts from volcanic rocks suggests either a brief interval between olivine crystallization and eruption or extremely sluggish diffusion, or some combination in between. Extended to

basalt liquidus temperatures, our Arrhenius law for P diffusion data in olivine places the diffusivity of this element at ~10^{-18} m^2/s—about an order of magnitude slower than Cr and Ca, and roughly an equal amount faster than oxygen and the rare earth elements (the latter according to Remmert et al. 2008 and Cherniak 2010; see Figure 7). Relatively speaking, then, P is a slow-diffusing element, but it does not appear to be virtually immobile in olivine at magmatic temperatures as is Si (Figure 7). This ranking seems consistent with the observations of Milman-Barris et al. (2008), who noted preservation of both P and Cr zoning in olivine phenocrysts, with the latter being more subdued. Given the diffusion law of Ito and Ganguly (2006) for Cr in olivine, post-formation "holding" times for the crystals characterized by Milman-Barris et al. (2008) must have been very brief for Cr zoning to survive at all—which would allow effective preservation of zoning in slower-diffusing P. The question is: How much time really did elapse between formation of zoning and eruption of the host lava? Here we explore the effects of isothermal holding on preservation of zoning.

Typical widths of the fine-scale P zoning features imaged by Milman-Barris et al. (2008) are on the order of ~5 μm; so we ran forward models beginning with tabular concentration anomalies of this dimension. The extent of 1-dimensional diffusive relaxation was computed for isothermal holding at 1150°, 1200° and 1250°C (relaxation during cooling is readily modeled, too; however, very fast cooling is implied by the fact that the modeled olivines are phenocrysts in eruptive rocks, so the cooling interval probably contributed little to any diffusive relaxation). In brief, the results (Figure 14) suggest that the olivine phenocrysts examined by Milman-Barris et al. (2009) and Welsch et al. (2014) generally cannot have spent more than a few months at magmatic temperatures prior to eruption. Longer durations at near-liquidus

478 temperatures for basaltic magmas would result in pronounced "damping" of 5µm-scale P
479 zoning. The implication seems to be that the olivine phenocrysts grew very shortly before
480 eruption of the host lavas, a suggestion supported by the preservation of zoning in faster-
481 diffusing Cr as well as P (see Ito and Ganguly 2006 for Cr data).

482 The P zoning profiles measured by Mallman et al. (2009) in olivines from metasomatized
483 spinel peridotite xenoliths have much larger characteristic lengths that those just described
484 from volcanic rocks—implying longer post-formation holding times and/or slow cooling. The
485 character of the P zoning includes concentric variation in a few large porphyroblasts (attributed
486 to diffusive relaxation following a metasomatic event), and more common patchy variations
487 created by physical deformation or recrystallization of concentrically zoned olivines during
488 events preceding the eruption of the host lavas. In an effort to reproduce two P analytical
489 traverses published by Mallman et al. (2009), we ran forward simulations of P diffusion at three
490 different temperatures using our new Arrhenius parameters, assuming sharp initial
491 concentration steps between high- and low-phosphorus regions. The simulations were run at
492 800°, 900° and 1000°C—chosen to encompass the ~870° to 950°C equilibration temperatures
493 of the xenoliths estimated by Mallman et al. (2009) on the basis of major-element phase
494 composition. The simulation results are shown in Figure 15 in comparison with LA/ICP-MS
495 traverses from Mallman et al. (2009). One of the profiles represents roughly concentric P
496 zoning across a ~7-mm diameter olivine porphyroblast, which was modeled as diffusion in a
497 sphere (Figure 15a); the other (Figure 15b) is a line traverse from a high- to low-concentration
498 patch within a single crystal, modeled as simple 1-D diffusion. For an isothermal holding period,
499 diffusion progress (as indicated by the shape of a partially-relaxed diffusion profile) is

500 determined by the product of the diffusivity (D) and time (t). The model profiles shown in
501 Figure 15 correspond to specific D·t values; D is known for the temperatures of interest, so for a
502 given temperature (800°, 900° or 1000°C) each model curve corresponds to a specific diffusion
503 time, as indicated on the figure. Suggested diffusion times for relaxation of the P profile in the
504 large olivine porphyroblast (Figure 15a) range from ~60 kyr at 1000°C to ~3 Myr at 800°C. If an
505 initial discontinuity in P concentration was created during a metasomatic event as suggested by
506 Mallman et al. (2009), then our estimates correspond to the time elapsed between the
507 metasomatic event and the eruption that brought the peridotite xenoliths to the surface
508 (assuming the initial profile was in fact a step).

509 Phosphorus diffusion from high- to low-P patches in smaller olivine crystals analyzed by
510 Mallman et al. (2009) appears to be much less advanced than in the large porphyroblasts
511 (Figure 15b). The 1-dimensional diffusion models shown in the figure suggest diffusion times
512 ranging from ~900 yr at 1000° to ~50 kyr at 800°C, but the "fit" is poorly constrained because
513 the data points are sparse. In principle, the estimated durations correspond to the time
514 elapsed between the subsolidus deformation event that juxtaposed high- and low-P olivine and
515 eruption of the host alkali basalt.

516 We have no basis for independent evaluation of the time estimates described above, but
517 the numbers seem plausible—especially if the metasomatic event recognized by Mallman et al.
518 (2009) was a close precursor to melt production and eruption. Realistically, of course, the
519 diffusion times we have estimated from P profiles are subject to large uncertainty, not least
520 because the starting profile is poorly known. An initial step discontinuity in concentration
521 seems reasonable for boundaries created by physical juxtaposition or partial recrystallization,

but is perhaps harder to defend in the case of initial profiles resulting from chemical interaction.

In the foregoing discussion of diffusive relaxation, the P concentration profiles reported by Mallman et al. (2009) were assumed to have developed during isothermal holding periods in the lithosphere. This choice was made simply for lack of more defensible scenarios, but there may be other instances in which diffusive relaxation can reasonably be assumed to have occurred mainly during cooling. For such cases, Watson and Cherniak (2015) provide simple equations for extracting cooling-rate information from partially relaxed ("stranded") diffusion profiles. The only quantity needed is an estimate of the slope (S_0) of the concentration profile, which is inserted into the equation

$$\log S_0 = 2.504 - \frac{1}{2}\log D_0 - \log T_i + \frac{1}{2}\log E_a + \frac{1}{2}\log \dot{T} + \left(26.11\frac{E_a}{T_i} \right), \qquad (2)$$

where D_0 and E_a are the Arrhenius parameters for the diffusant of interest (m^2/s and kJ/mol, respectively), T_i is the initial temperature (kelvins), and is the linear cooling rate (°/s). The slope (S_0) of the profile of interest is estimated at the midpoint of the interdiffusion profile, with concentrations normalized to a difference of 100 between the upper (= 100) and lower (= 0) concentration extremes; distance is expressed in m. If we assume, for demonstration purposes, that the profile shown in Figure 15b developed entirely during cooling from an initial temperature of 900°C, our method would yield a cooling-rate estimate of ~ 0.008°/yr.

CONCLUDING REMARKS

Our newly determined Arrhenius parameters for lattice diffusion of P in olivine qualify this element as a slow diffuser relative to divalent cations of radius similar to or smaller than that of

Ca (including Fe and Mg). At 1300°C, our estimated diffusivity of 2×10^{-18} m^2/s is at the edge of consistency with the maximum permissible value of Spandler et al. (2007), which is based on a laboratory attempt to diffusively "blur" P zoning in a natural olivine crystal. On the other hand, P diffuses in olivine about 3 orders of magnitude faster than Si at temperatures near the basalt liquidus, which means that P zoning features cannot be regarded as immoveable markers for all intents and purposes. The modest mobility of P raises the possibility of using measured P concentration profiles to estimate T-t histories of host olivines, as noted by Milman-Barris et al. (2008). Applied to the spinel peridotite samples described by Mallman et al. (2009), this approach suggests a geologically short time interval (a few hundred thousand years) between a precursor mantle metasomatic event and alkali basalt eruption. Our diffusion law for P in olivine suggests that the fine-scale zoning documented extensively by Milman-Barris et al. (2008) and Welsch et al. (2014) in olivine phenocrysts was formed only days to months before eruption. It must be borne in mind, however, that these simple calculations do not consider the possibility of multi-stage T-t histories. Phosphorus zoning on the phenocryst scale can be preserved for protracted time periods at subsolidus temperatures, a fact that is readily appreciated from the Dodson (1973) closure temperatures (T_C) implied by our Arrhenius law. For an olivine grain of 0.5 mm radius, T_C ranges from 984°C for a cooling rate of 0.01 °/yr to 630°C for a cooling rate of 10^{-6} °/yr. Although T_C is not useful in describing relaxation of fine-scale zoning (as in Figure 14), it does convey a general sense of the conditions that must be met in order to "lock in" zoning at a particular scale—in this case an entire grain of 0.5 mm radius.

Knowledge of P lattice diffusion in olivine makes it possible to evaluate kinetic influences that might be involved in the formation of P zoning in olivine, one of which is the growth

565 entrapment model (GEM) of Watson and Liang (1995). In this model, local concentrations of
566 impurities in crystals higher than the equilibrium partitioning value owe their existence to
567 "capture" of a near-surface chemical anomaly during crystal growth, as a consequence of fast
568 growth and/or sluggish lattice diffusion. The lattice diffusion data presented here indicate that
569 growth entrapment of P in olivine is likely at geologically plausible rates for sustained olivine
570 growth, and a brief interval of accelerated growth could result in zoning that appears in 2-D
571 section to be oscillatory in nature (see Welsch et al. 2013; 2014).

572 Our diffusion results for MORB basalt melt indicate that the diffusivity of P is similar to
573 that of Si, and about an order of magnitude faster than Baker's (2008) characterization of P
574 diffusion in molten hawaiite. Phosphorus diffuses sufficiently slowly to lead to its enrichment in
575 a diffusive boundary layer against a rapidly growing olivine, but growth rates that are
576 unrealistically high for sustained growth are needed to produce a large effect (that is,
577 enrichment of P in olivine to values more than 10-20% above equilibrium levels). Brief episodes
578 of olivine growth at dendrite-forming rates could nevertheless lead to several-fold local
579 enrichment of P in the resulting crystals. In general, the influence of a P diffusive boundary
580 layer in the melt seems unlikely to be as efficient in causing non-equilibrium P uptake in olivine,
581 simply because diffusion of Si must itself limit the growth rate of olivine (and Si and P have
582 similar diffusivities in the melt, according to our data). For this reason we favor a kinetic effect
583 in the crystal itself (in the form of growth entrapment) as the more likely cause of P zoning in
584 olivine. As noted previously, this is essentially required for the development of sector zoning.

585 **Acknowledgements**. This work was supported by NSF grant EAR-0738843 to E.B.W.

586

REFERENCES

Ahmad, N.A., Wheeler, A.A., Boettinger, W.J. and McFadden, G.B. (1998) Solute trapping and solute drag in a phase-field model for rapid solidification. Phys. Rev. E, 58, 3436–3450.

Albarède, F. and Bottinga, Y. (1972) Kinetic disequilibrium in trace-element partitioning between phenocrysts and host lava. Geochim Cosmochim Acta, 36, 141–156.

Aziz, M.J. (1982) Model for solute redistribution during rapid solidification. J. Appl. Phys., 53, 1158–1168.

Aziz, M.J. (1984) Crystal Growth and Solute Trapping. Materials Research Society Symposium Proceedings, 23, 369-374.

Aziz, M.J. (1996) Interface attachment kinetics in alloy solidification. Metall. Mat. Trans. A, 27**,** 671–685.

Bacon, C.R. (1989) Crystallization of accessory phases in magmas by local saturation adjacent to phenocrysts. Geochim Cosmochim Acta, 53, 1055–1066.

Baker, D.R. (2008) The fidelity of melt inclusions as records of melt composition. Contrib. Mineral. Petrol., 156, 377-395.

Catalano, J. G., Fenter, P. and Park, C. (2009) Water ordering and surface relaxations at the hematite (110)-water interface. Geochim. Cosmochim. Acta, 73, 2242–2251.

Chakraborty, S. (1997) Rates and mechanisms of Fe–Mg interdiffusion in olivine at 980–1300. J. Geophys. Res., 102, 12317–12331.

606 Chakraborty, S. (2010) Diffusion coefficients in olivine, wadsleyite and ringwoodite. In: *Diffusion*
607 *in Minerals and Melts*, Reviews in Mineralogy and Geochemistry 72 (Y Zhang and DJ
608 Cherniak, Eds.), Mineralogical Society of America, pp. 603-639.

609 Chen, Y. and Zhang, Y. (2008) Olivine dissolution in basaltic melt. Geochim. Cosmochim. Acta,
610 72, 4756-4777.

611 Chen, Y. and Zhang, Y. (2009) Clinopyroxene dissolution in basaltic melt. Geochim. Cosmochim.
612 Acta, 73, 5730-5747.

613 Cherniak, D.J. (2010) REE diffusion in olivine. Am. Mineral., 95, 362-368.

614 Cherniak, D.J. (1995) Sr and Nd diffusion in titanite. Chemical Geology, 125, 219-232.

615 Cherniak, D.J. (2010) REE diffusion in olivine. Am. Mineral., 95, 362-368.

616 Cherniak, D.J. and Lanford, W.A. (2001) Nuclear Reaction Analysis. In: Non-Destructive
617 Elemental Analysis. Alfassi Z. (ed.) Blackwell Science, pp 308-338.

618 Cherniak, D.J. and Watson, E.B. (1994) A study of strontium diffusion in plagioclase using
619 Rutherford Backscattering Spectroscopy. Geochim. Cosmochim. Acta, 58, 5179-5190.

620 Cherniak, D.J., Thomas, J.B. and Watson, E.B. (2014) Neon diffusion in olivine and quartz.
621 Chemical Geology, 371, 68-82.

622 Cherniak, D.J., Watson, E.B. and Wark, D.A. (2007) Ti Diffusion in quartz. Chemical Geology,
623 236, 65-74.

Coogan, L., Hain, A., Stahl, S. and Chakraborty, S. (2005) Experimental determination of the diffusion coefficient for Ca in olivine between 900°C and 1500°C. Geochim. Cosmochim. Acta, 69, 3683-3694.

Demouchy, S. and Mackwell, S.J. (2003) Water diffusion in synthetic iron-free forsterite. Phys. Chem. Miner., 30, 486-494.

Demouchy, S. and Mackwell, S.J. (2006) Mechanisms of hydrogen incorporation and diffusion in iron-bearing olivine. Phys. Chem. Miner., 33, 347-355.

Dodson, M.H. (1973) Closure temperature in cooling geochronological and petrological systems. Contrib. Mineral. Petrol., 40, 259-274.

Dohmen, R., Chakraborty, S. and Becker, H.W. (2002) Si and O diffusion in olivine and implications for characterizing plastic flow in the mantle. Geophys. Res. Lett., 29. doi:10.1029/2002GL015480.

Dohmen, R., Kaseman, S., Coogan, L. and Chakraborty, S. (2010) Diffusion of Li in olivine I: Experimental observations and multispecies diffusion model. Geochim. Cosmochim. Acta, 74, 274-292.

Dowty, E. (1977) The importance of adsorption in igneous partitioning of trace elements. Geochim. Cosmochim. Acta, 41, 1643–1646.

Fenter, P., Geissbuhler, P., DiMasi E., Srajer G., Sorensen L. B. and Sturchio N. C. (2000a) Surface speciation of calcite observed in situ by high-resolution X-ray reflectivity. Geochim. Cosmochim. Acta, 64, 1221–1228.

644 Fenter, P., Teng, H., Geissbuhler, P., Hanchar, J.M., Nagy, K.L. and Sturchio, N.C. (2000b)
645 Atomic-scale structure of the orthoclase (001)-water interface measured with high-
646 resolution X-ray reflectivity. Geochim. Cosmochim. Acta, 64, 3663–3673.

647 Fenter, P., McBride, M.T., Srajer, G., Sturchio, N.C. and Bosbach, D. (2001) Structure of barite
648 (001)- and (210)-water interfaces. J. Phys. Chem. B, 105, 8112–8119.

649 Fenter, P., Cheng, L., Park, C., Zhang, Z. and Sturchio, N.C. (2003) Structure of the orthoclase
650 (001)- and (010)-water interfaces by high-resolution X-ray reflectivity. Geochim.
651 Cosmochim. Acta, 67, 4267–4275.

652 Galenko, P.K. (2002) Extended thermodynamical analysis of a motion of the solid-liquid
653 interface in a rapidly solidifying alloy. Phys. Rev. B, 65, art. no. 144103.

654 Gerard, O. and Jaoul, O. (1989) Oxygen diffusion in San Carlos olivine. J. Geophys. Res. [Solid
655 Earth], 94, 4119-4128.

656 Green, T.H. and Watson, E.B. (1982) Crystallization of apatite in natural magmas under high-
657 pressure, hydrous conditions, with particular reference to 'orogenic' rock series. Contrib.
658 Mineral. Petrol., 79, 96-105.

659 Harrison, T.M. and Watson, E.B. (1984) The behavior of apatite during crustal anatexis:
660 Equilibrium and kinetic considerations. Geochim. Cosmochim. Acta, 48, 1467-1477.

661 Houlier, B., Cheraghmakani, M. and Jaoul, O. (1990) Silicon diffusion in San Carlos olivine. Phys.
662 Earth Planet. Int., 62, 329-340.

Ito, M. and Ganguly, J. (2006) Diffusion kinetics of Cr in olivine and ^{53}Mn-^{53}Cr thermo-chronology of early solar system objects. Geochim. Cosmochim. Acta, 70, 799-809.

Jambon, A., Lussiez, P. and Clocchiatti, R. (1992) Olivine growth rates in a tholeiitic basalt: An experimental study of melt inclusions in plagioclase. Chem. Geol., 96, 277-287.

Kohlstedt, D.L. and Mackwell, S.J. (1998) Diffusion of hydrogen and intrinsic point defects in olivine. Zeit. Phys. Chem., 207, 147-162.

Lanzillo, N.A., Watson, E.B., Thomas, J.B., Nayak, S.K. and Curioni, A. (2014) Near-surface controls on the composition of growing crystals: Car-Parrinello molecular dynamics (CPMD) simulations of Ti energetics and diffusion in alpha quartz. Geochim. Cosmochim. Acta, 131, 33-46. DOI: 10.1016/j.gca.2014.01.015.

Lebedev, V.G., Abramova, E.V., Danilov, D.A. and Galenko, P.K. (2010) Phase-field modeling of solute trapping: comparative analysis of parabolic and hyperbolic models. Int. J. Mat. Res. (formerly Z. Metallkd.), 101, 473-479.

Lesher, C.E., Hervig, R.L. and Tinker, D. (1996) Self-diffusion of network-formers (silicon and oxygen) in naturally-occurring basaltic liquid. Geochim. Cosmochim. Acta, 60, 405-413.

Lesher, C.E. and Walker, D. (1986) Solution properties of silicate liquids from thermal diffusion experiments. Geochim. Cosmochim. Acta, 50, 1397-1411.

Lundstrom, C.C. (2003) An experimental investigation of the diffusive infiltration of alkalis into partially molten peridotite: implications for mantle melting processes. Geochem. Geophys. Geosys., 4. doi: 10.1029/2001GC000224.

Maaloe, S. (2011) Olivine phenocryst growth in Hawaiian tholeiites: evidence for supercooling. J. Petrol., 52, 1579-1589.

Mallman, G., O'Neill, H. StC. and Klemme, S. (2009) Heterogeneous distribution of phosphorus in olivine in otherwise well-equilibrated spinel peridotite xenoliths and its implications for the mantle geochemistry of lithium. Contrib. Mineral. Petrol., 158, 485-504. doi 10.1007/s00410-009-0393-6.

McIntyre, jr., L.C., Leavitt, J.A., Dezfouly-Arjomady, B. and Oder, J. (1988) Depth profiling of phosphorus using resonances in the $^{31}P(\alpha,p)^{34}S$ reaction. Nuclear Instruments and Methods, B35, 446-450.

McKibbin, S.J., O'Neill, H. StC., Mallman, G. and Halfpenny, A. (2013) LA-ICP-MS mapping of olivine from the Brahin and Brenham meteorites: Complex elemental distributions in the pallasite olivine precursor. Geochim. Cosmochim. Acta, 119, 1-17.

Milman-Barris, M., Beckett, J., Baker, M., Hofmann, A., Morgan, Z., Crowley, M., Vielzeuf, D. and Stolper, E. (2008) Zoning of phosphorus in igneous olivine: Contrib. Mineral. Petrol., 155, 739–765. doi: 10.1007 /s00410 -007-0268-7.

Pitters, J.L., Piva, P.G. and Wolkow, R.A. (2012) Dopant depletion in the near surface region of thermally prepared silicon (100) in UHV. J. Vac. Sci. Technol., B, 30, 021806.

Remmert, P., Dohmen, R. and Chakraborty, S. (2008) Diffusion of REE, Hf and Sr in olivine. EOS Trans. AGU, 89, MR33A-1844.

Ryerson, F.J., Durham, W.B., Cherniak, D.J. and Lanford, W.A. (1989) Oxygen diffusion in olivine -- effect of oxygen fugacity and implications for creep. J. Geophys. Res. [Solid Earth], 94, 4105-4118.

Sakyi, P. A., Tanaka, R., Kobayashi, K. and Nakamura, E. (2012). Inherited Pb isotopic records in olivine antecryst-hosted melt inclusions from Hawaiian lavas. Geochem. Geophys. Geosyst., 95, 169-195.

Sautter, V., Jaoul, O. and Abel, F. (1988) Aluminum diffusion in diopside using the $^{27}Al(p,\gamma)^{28}Si$ nuclear reaction: preliminary results. Earth Planet Sci Lett, 89, 109-114.

Schlegel, M. L., Nagy, K. L., Fenter, P. and Sturchio, N. C. (2002) Structures of quartz ($10\bar{1}0$) and ($10\bar{1}1$) water interfaces determined by X-ray reflectivity and atomic force microscopy of natural growth surfaces. Geochim. Cosmochim. Acta, 66, 3037-3054.

Schmoluchowski, M. v. (1915) Über Brownsche Molekularbewegung unter Einwirkung äußerer Kräfte und deren Zusammenhang mit der verallgemeinerten Diffusionsgleichung. Annalen der Physik, 48, 1103-1112.

Smith, V.G., Tiller, W.A. and Rutter, J.W. (1955) A mathematical analysis of solute redistribution during solidification. Can. J. Phys., 33, 723–745.

Spandler, C. and O'Neill, H. StC. (2009) Diffusion and partition coefficient of minor and trace elements in San Carlos olivine at 1300°C with some geochemical implications. Contrib. Mineral. Petrol., 159, 791-818.

Spandler, C., O'Neill, H. StC. and Kamenetsky, V.S. (2007) Survival times of anomalous melt

722 inclusions from element diffusion in olivine and chromite. Nature, 447, 303-306.
723 doi:10.1038/nature05759.

724 Tiller, W.A. and Ahn, K.-S. (1980) Interface field effects on solute redistribution during
725 crystallization. J. Crystal Growth, 49, 483–501.

726 Tiller, W.A., Jackson, K.A., Rutter, J.W. and Chalmers, B. (1953) The redistribution of solute
727 atoms during the solidification of metals. Acta Metallurgica, 1, 428-437.

728 Tschegg, C., Ntaflos, T., Kiraly, F. and Harangi, S. (2010). High temperature corrosion of olivine
729 phenocrysts in Pliocene basalts from Banat, Romania. Aust. J. Earth Sci., 103, 101-110.

730 Watson, E.B. (1996) Dissolution, growth and survival of zircons during crustal fusion: Kinetic
731 principles, geologic models and implications for isotopic inheritance. Proc. Roy. Soc.
732 Edinburgh, 87, 43-56.

733 Watson, E.B. (2004) A conceptual model for near-surface kinetic controls on the trace-element
734 and stable-isotope composition of abiogenic calcite. Geochim. Cosmochim. Acta, 68, 1473-
735 1488.

736 Watson E.B., Wark D.A., Price, J.D. and Van Orman, J.A. (2002) Mapping the thermal structure
737 of solid-media pressure assemblies. Contrib. Mineral. Petrol., 142, 640-652.

738 Watson, E.B. and Cherniak, D.J. (2015) Quantitative cooling histories from stranded diffusion
739 profiles. Contrib. Mineral. Petrol. (in revision May, 2015).

740 Watson, E.B. and Dohmen, R. (2010) Non-traditional and emerging methods for diffusion

measurements. In: Diffusion in Minerals and Melts (Y. Zhang and D. Cherniak, Eds.) *Reviews in Mineralogy and Geochemistry*, Mineralogical Society of America. DOI: 10.2138/rmg.2010.72.3.

Watson, E.B. and Harrison, T.M. (1984) Accessory minerals and the geochemical evolution of crustal magmatic systems: a summary and prospectus of experimental approaches. Phys. Earth Planet. Int., 35, 19-30.

Watson, E.B. and Liang, Y. (1995) A simple model for sector zoning in slowly-grown crystals: Implications for growth rate and lattice diffusion, with emphasis on accessory minerals in crustal rocks. Am. Mineral., 80, 1170-1187.

Watson, E.B. and Müller, T. (2009) Non-equilibrium isotopic and elemental fractionation during diffusion-controlled crystal growth under static and dynamic conditions. Chem. Geol., 267, 111-124 doi:10.1016/j.chemgeo.2008.10.036.

Welsch, B., Faure, F., Famin, V., Baronnet, A. and Bachèlery, P. (2013). Dendritic crystallization: A single process for all the textures of olivine in basalts? J. Petrol., 54, 539-574.

Welsch, B., Hammer, J. and Hellebrand, E. (2014) Phosphorus zoning reveals dendritic architecture of olivine. Geology, 42, 867-870. doi: 10.1130/G35691.1.

Zhang, Z., Fenter, P., Sturchio, N.C., Bedzyk, M.J., Machesky, M.L. and Wesolowski, D.J. (2007) Structure of rutile TiO_2 (110) in water and 1 molal Rb+ at pH 12: inter-relationship among surface charge, interfacial hydration structure, and substrate structural displacements. Surf. Sci., 601, 1129–1143.

761 Ziegler, J.F. and Biersack, J.P. (2006) The stopping and range of ions in matter. Computer code
762 SRIM 2006, http://www.srim.org.

763

764 **Figure captions**

765 Figure 1. Schematic of experimental setup for phosphorus diffusion experiments on San Carlos
766 olivine. The P source indicated was pre-reacted in vacuo at 900°C for 16h. This source was used
767 for all but one experiment; the exception involved a pre-reacted 60:40 mix of ground San Carlos
768 lherzolite with $AlPO_4$. See text for discussion.

769 Figure 2. Schematic of piston-cylinder assembly used for P diffusion experiments on basaltic
770 melt.

771 Figure 3. Top panels: Representative diffusion profiles for phosphorus in San Carlos olivine
772 measured by Rutherford backscattering spectroscopy (RBS). Bottom panels show the raw data
773 from the top panels linearized by inversion through the error function to obtain the diffusivity
774 from the slope. C_0 is the P concentration at the sample surface. See text for more details.

775 Figure 4. Phosphorus diffusion profiles in basaltic melt characterized by LA-ICP/MS analysis of
776 quenched glasses. These examples were selected to represent the full range in temperature of
777 this study (1250-1500°C); run conditions are indicated on each panel. The smooth gray curves
778 are fits of the data to the equation shown on the figure, with the upper and lower
779 concentration plateaus and the diffusivity (D) as free parameters. Run 18 is essentially a zero-
780 time experiment, the results of which confirm that the initial P profiles in the experiments are
781 steps. The diffusivity calculated from run 18 is not meaningful, even though it is in general
782 agreement with results from other experiments at 1300°C (see time series in Figure 8).

783 Figure 5. Arrhenius-type summary of measured diffusion coefficients for phosphorus in San

Carlos olivine (SCO). All but two experiments were run with a nickel-nickel oxide (NNO) oxygen buffer (exceptions are white circles, run at wüstite-magnetite). Note that diffusivities were obtained for two crystallographic directions; "pdt" refers to one experiment in which the SCO was surrounded by a powder containing the full San Carlos mineral assemblage rather than just orthopyroxene as in the rest of the experiments (see text and Figure 1). Error bars are $\pm 2\sigma$; these come from the uncertainties in the fits of measured P profiles to the constant-surface diffusion model (see text and Figure 3).

Figure 6. Results of a time series of four olivine diffusion experiments at 825°C confirming that the P diffusivity is independent of experiment duration over a wide range in time. Symbols as in Figure 5.

Figure 7. Summary of published diffusion laws for a variety of elements in comparison with the new data for P. Note the near coincidence between the maximum estimate for P diffusivity at 1300°C from Spandler et al. (2007) with the up-temperature extrapolation of the Arrhenius law determined in the present study. Shaded fields encompass multiple Arrhenius lines from two or more research groups. The large field for Fe-Mg interdiffusion includes 8 different studies summarized by Chakraborty (2010); the vertical spread in this case is due mainly to f_{O2} effects. Other data sources:

Si: Dohmen et al. (2002); Houlier et al. (1990)

O: Ryerson et al. (1989); Dohmen et al. (2002); Gerard and Jaoul (1989)

REE: Spandler et al. (2007); Remmert et al. (2008); Cherniak (2010)

Cr: Ito and Ganguly (2006); Spandler and O'Neill (2010)

Ca: Coogan et al. (2005)

Li: Dohmen et al. (2010)

V_{Me} (metal vacancies): Kohlstedt and Mackwell (1998)

H: Demouchy and Mackwell (2003; 2006)

Figure 8. Summary of P diffusion data for MORB melt determined in this study (black squares) in comparison with previous results for P and Si in dry melts of broadly basaltic composition (48.5 ± 2.6 wt% SiO_2); see legend for data sources. Note that the P data from the present study are nearly indistinguishable from some previous determinations for Si. The error bars on the individual data points represent $\pm$ 2 s.e. based in the quality of the fits to the individual diffusion profiles (Figure 4). The overall experimental reproducibility can be evaluated from the four experiments at 1300°C. A linear fit to the new data yields Arrhenius parameters as follows: $\log(D_0, m^2/s) = -6.30 \pm 0.7$ and $E_a = 147 \pm 22$ kJ/mol. EBD = Effective Binary Diffusion.

Figure 9. Phosphorus diffusion results from a time series of five experiments on basaltic melt at 1300°C. Note that the briefest experiment (no. 18) was only 90s in duration (essentially a zero-time run); this resulted in large uncertainty in the diffusivity recovered from this experiment, the main goal of which was to demonstrate that the initial concentration profile is a step (see Figure 4).

Figure 10. Model curves showing enrichment of P in (and against) olivine crystals in response to brief periods of rapid growth from basaltic melt at three different speeds: $V = 10^{-8}$, 10^{-7} and 10^{-6} m/s. The initial spherical olivine crystal was assigned a radius r_0 of 500 µm and allowed to grow by 10 µm (see inset), mimicking the scale of fine P zoning in natural olivine phenocrysts (the

826 distances shown are microns from the center of the olivine crystal). The equilibrium
827 olivine/melt partition coefficient was assumed to be 0.1; the initial P concentration in the melt
828 was taken as 1000 ppm, but this can be adjusted to any preferred value and other
829 concentrations scaled accordingly. (**a**) Phosphorus concentration profile across the 10 μm of
830 new olivine growth; (**b**) phosphorus pileup in advance of the moving interface for the same
831 three scenarios. All profiles were computed numerically using the moving-boundary algorithm
832 for spherical geometry described by Watson and Müller (2009). The P diffusivity in the melt
833 used in the calculations was that given by our new Arrhenius equation at 1215°C ($D = 3.5 \times 10^{-12}$
834 m^2/s); P was assumed to be immobile in olivine for the brief growth events portrayed.

835 Figure 11. Hypothetical equilibrium concentration anomaly in the near-surface of a crystal
836 lattice (e.g., P in olivine) resulting from structural relaxation of atoms from their normal lattice
837 positions. C_i is the concentration at distance coordinate z, which decreases from a value of zero
838 at the surface. C_{eq} is the equilibrium concentration in the bulk lattice; F_S is the equilibrium
839 concentration ratio at the surface relative to the bulk lattice, analogous to a surface partition
840 coefficient; l is the half-width of the chemically anomalous layer. See text for more details.

841 Figure 12. Schematic illustration of the phenomenon of growth entrapment, where the near-
842 surface concentration anomaly (Figure 11) is "captured" with varying efficiency during growth
843 of the crystal. See Figure 13 for quantitative calculations of this effect.

844 Figure 13. Growth entrapment results based on numerical solution of equation 1 using the
845 lattice diffusivity of P in olivine determined in this study (and F_S = 10; l = 0.5 nm). The olivine
846 growth rate, V, is the linear rate of advancement of the crystal/melt interface. The likely realm

847 of sustained V for phenocrysts in natural systems indicated by the shaded region (Maaloe
848 2011); however, faster, dendrite-forming growth "spurts" are also possible (Jambon et al.
849 1992). The high extreme of the shaded region ($V \sim 5\times10^{-9}$ m/s) pertains to growth of settling
850 olivine crystals in a convecting system that is undercooled by 40°C. Note that growth trapping
851 effectiveness increases with decreasing temperature because of slower diffusion in the olivine
852 near-surface. See text for details.

853 Figure 14. Progressive relaxation of an initial 5-micron wide P concentration anomaly in olivine
854 at 1250°, 1200° and 1150°C. In each panel, the initial feature is the tall rectangle with a
855 concentration of 100 ppm above a background concentration of 20 ppm. Each bell-shaped
856 curve represents an incremental diffusion time of 1 year, up to a maximum time of 10 years.
857 See text for discussion.

858 Figure 15. (**a**) Computed profiles in a spherical diffusion field resulting from isothermal
859 relaxation of an initial step profile in P concentration (dashed). The goal in computing these
860 profiles was to obtain a general match with broad, concentric zoning in an olivine porphyroblast
861 from a spinel peridotite xenolith described by Mallman et al. (2009; black circles). Each curve
862 represents a specific value of Dt, but because D depends on temperature, the time elapsed
863 between the curves also depends on temperature, as indicated in the inset. The heavier black
864 curve is the best (visual) match; the diffusion time to reach this curve from the initial step
865 distribution is shown in the inset for 800°, 900° and 1000°C. (**b**) One-dimensional diffusive
866 relaxation model curves seeking similarity to a P profile reported by Mallman et al. (2009; black
867 circles) for a recrystallized olivine grain in a spinel peridotite xenolith. As in (a), each curve

868 represents diffusion progress in terms of a specific value of Dt; the relevant time depends on
869 temperature, as indicated in the inset. The "fit" is clearly poorly constrained because of data
870 sparsity; the black curve could be taken as the best result. See text for further discussion.

871

Table 1a. P diffusion in San Carlos olivine

	T(°C)	*time(sec)*	*D(m^2sec^{-1})*	*log D*	*σ*
Diffusion parallel to b					
P-*Ol*-1	800	6.19×10^{5}	6.63×10^{-22}	-21.18	0.13
P-*Ol*-3	850	1.18×10^{6}	2.48×10^{-21}	-20.61	0.11
P-*Ol*-4	750	1.18×10^{6}	1.69×10^{-22}	-21.77	0.24
P-Ol-5	700	6.15×10^{6}	3.08×10^{-23}	-22.51	0.36
P-*Ol*-6	650	6.15×10^{6}	1.08×10^{-23}	-22.96	0.42
P-*Ol*-7	675	3.84×10^{6}	2.49×10^{-23}	-22.60	0.25
P-*Ol*-8	725	3.84×10^{6}	8.03×10^{-23}	-22.10	0.12
P-*Ol*-9	825	8.51×10^{5}	8.15×10^{-22}	-21.09	0.14
P-*Ol*-10	775	8.51×10^{5}	3.77×10^{-22}	-21.42	0.13
P-*Ol*-15	825	2.88×10^{5}	1.29×10^{-21}	-20.89	0.11
P-*Ol*-16	825	2.40×10^{6}	8.70×10^{-22}	-21.06	0.14
P-*Ol*-WM1*	650	5.86×10^{6}	1.63×10^{-23}	-22.79	0.34
P-*Ol*-WM2*	816	9.31×10^{5}	1.78×10^{-21}	-20.75	0.16
P-*Ol*-per-1†	850	5.15×10^{5}	1.27×10^{-21}	-20.89	0.22
diffusion parallel to c					
P-*Ol*-11	800	1.03×10^{6}	2.99×10^{-22}	-21.52	0.12
P-*Ol*-12	825	2.51×10^{5}	1.20×10^{-21}	-20.92	0.12

Note: Experiments were buffered at Ni-NiO except for those marked with an asterisk (*), which were buffered at wüstite-magnetite.

† peridotite $AlPO_4$ source (see text)

Table 1b. P diffusion in basaltic melt

Run	*T(°C)*	*time (sec)*	*D(m^2sec^{-1})*	*log D*	*σ*
15	1300	1800	9.28×10^{-12}	-11.03	0.03
16	1350	1800	8.53×10^{-12}	-11.07	0.02
17	1275	2700	5.75×10^{-12}	-11.24	0.04
18	1300	90	6.98×10^{-12}	-11.16	0.33
22	1375	1800	9.58×10^{-12}	-11.02	0.03
24	1300	5400	6.11×10^{-12}	-11.21	0.03
27	1400	2100	1.14×10^{-11}	-10.94	0.05
28	1300	500	7.85×10^{-12}	-11.11	0.05
29	1300	1800	4.40×10^{-12}	-11.36	0.03
30	1500	1680	2.51×10^{-11}	-10.60	0.04
31	1500	1680	2.61×10^{-11}	-10.58	0.04
32	1400	2100	1.39×10^{-11}	-10.86	0.04
33	1250	3000	4.52×10^{-12}	-11.34	0.06

Watson et al. – Figure 1.

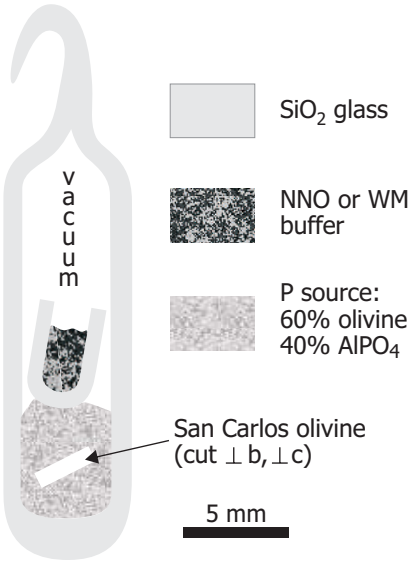

Watson et al. – Figure 2.

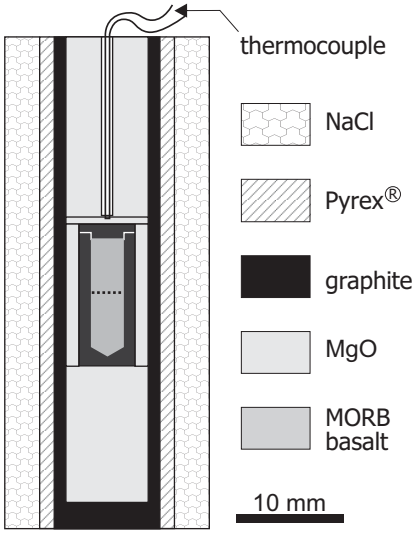

Watson et al. – Figure 3.

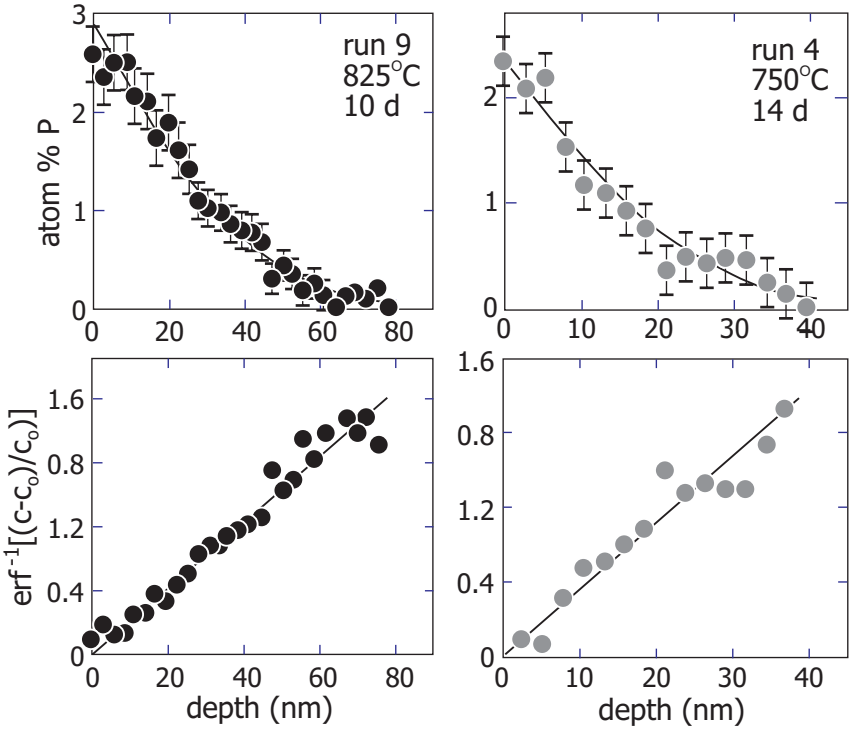

Watson et al. – Figure 4.

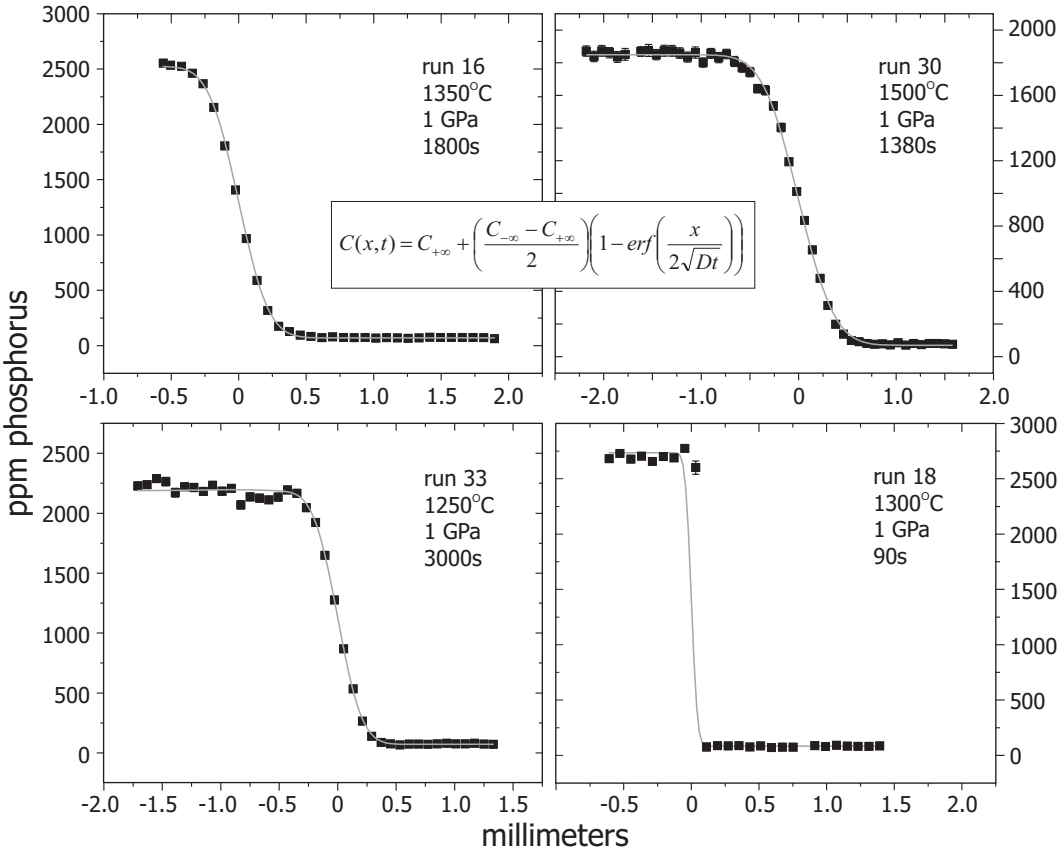

Watson et al. – Figure 5.

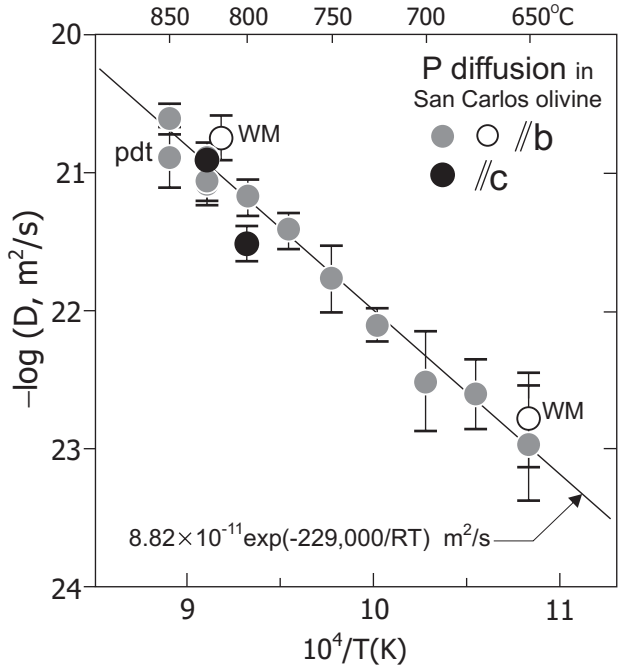

Watson et al. – Figure 6.

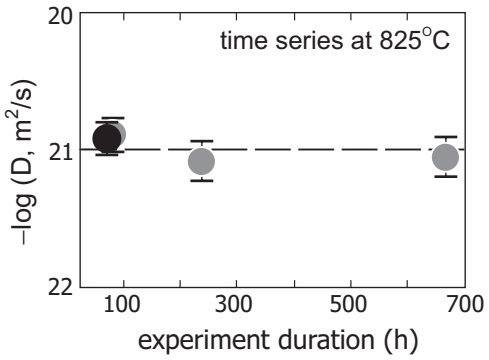

Watson et al. – Figure 7.

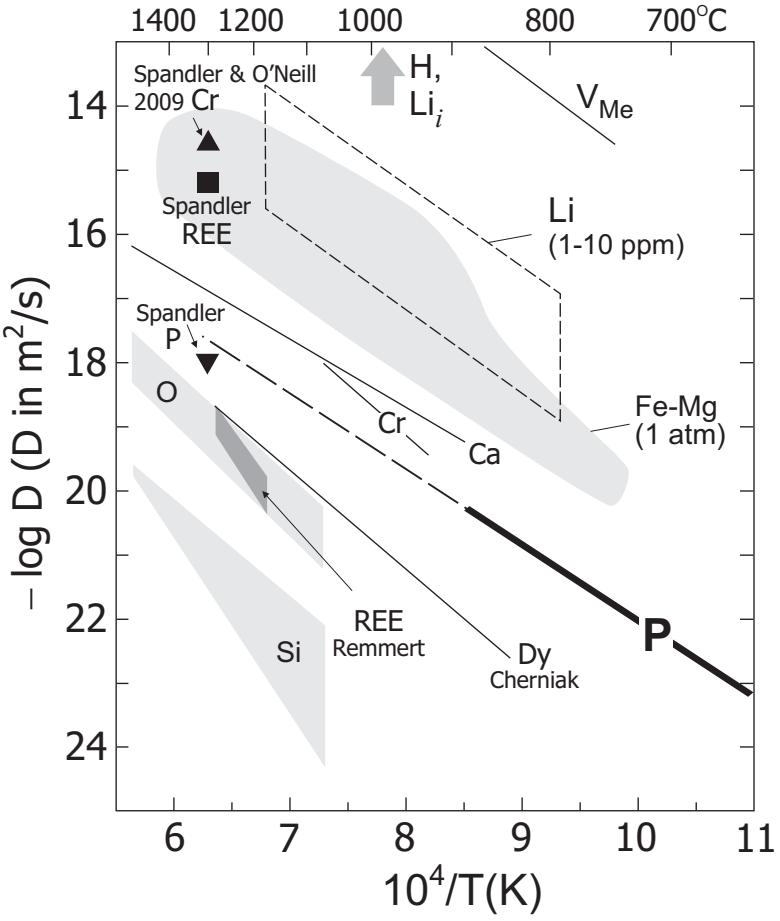

Watson et al. – Figure 8.

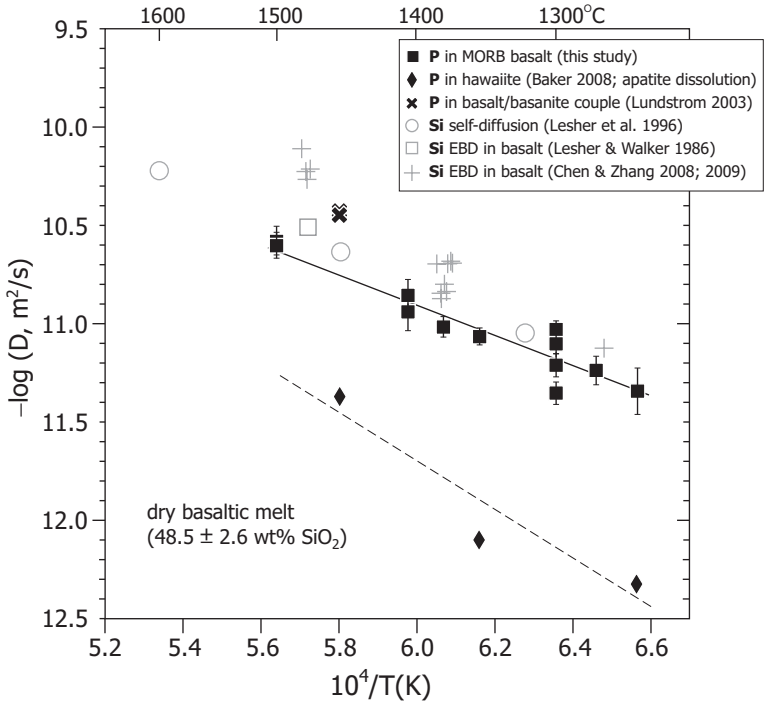

Watson et al. – Figure 9.

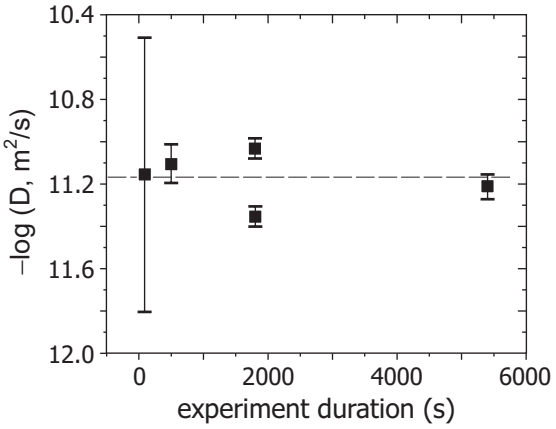

Watson et al. – Figure 10.

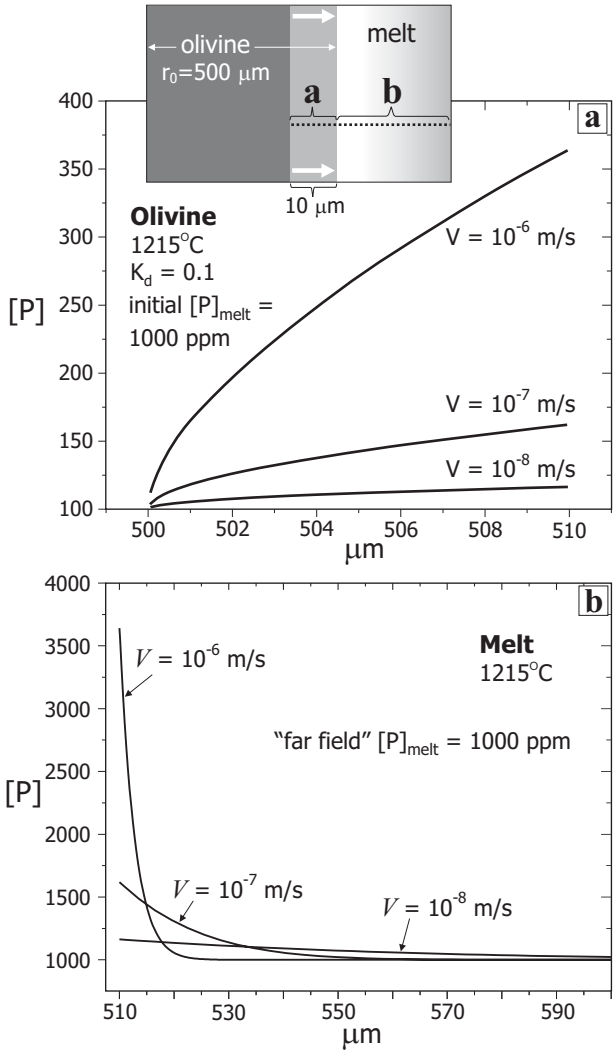

Watson et al. – Figure 11.

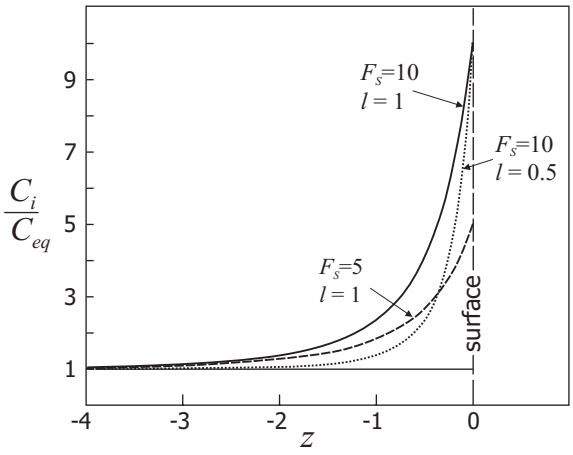

Watson et al. – Figure 12.

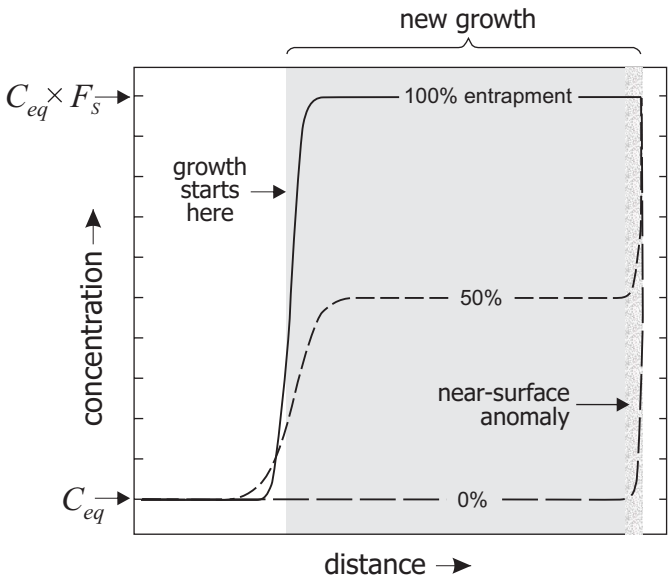

Watson et al. – Figure 13.

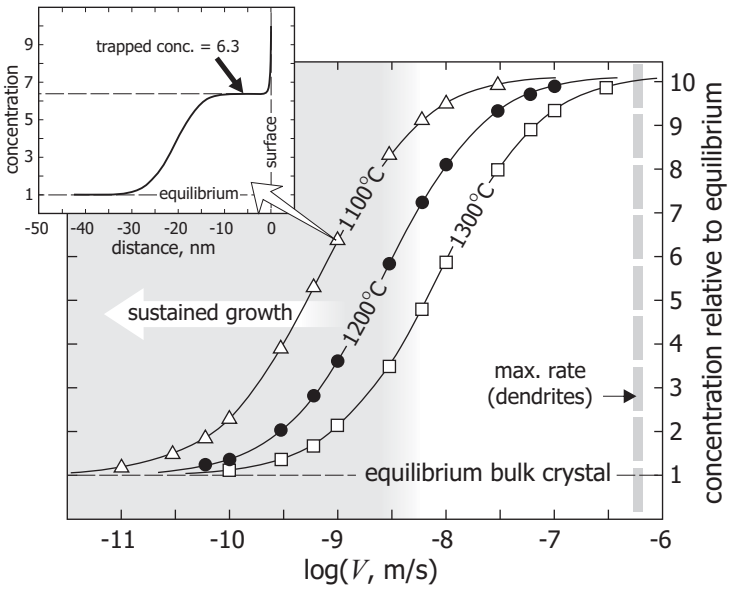

Watson et al. – Figure 14.

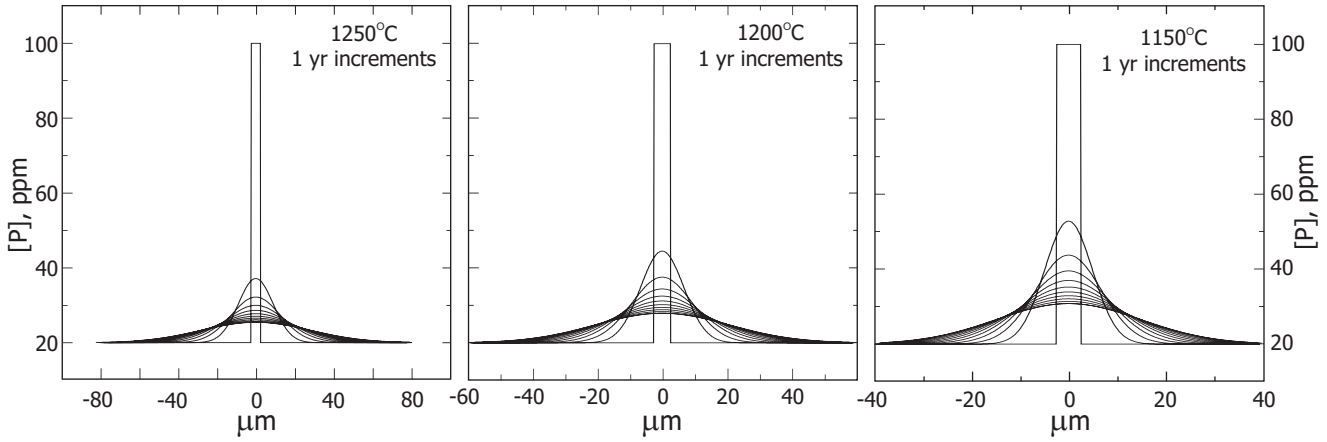

Watson et al. – Figure 15.